catalysts

MDPI

Article

The Denitration and Dedusting Behavior of Catalytic Filter and Its Industrial Application in Glass Kilns

Lin Huangfu [1,2], Zhaohui Chen [1], Changming Li [1,3,*], Xiaolong Yao [3], Zhiliang Yao [3], Guangwen Xu [4], Shiqiu Gao [1], Xing Huang [5] and Jian Yu [1,*]

1 State Key Laboratory of Multi-Phase Complex Systems, Institute of Process Engineering, Chinese Academy of Sciences, Beijing 100190, China; l_huangfu@163.com (L.H.); chenzh8i@163.com (Z.C.); sqgao@ipe.ac.cn (S.G.)
2 School of Chemical Engineering, University of Chinese Academy of Sciences, Beijing 100049, China
3 State Environmental Protection Key Laboratory of Food Chain Pollution Control, School of Ecology and Environment, Beijing Technology and Business University, Beijing 100048, China; yaoxiaolong@btbu.edu.cn (X.Y.); yaozhl@th.btbu.edu.cn (Z.Y.)
4 School of Chemical Engineering, Shenyang University of Chemical Technology, Shenyang 110142, China; gwxu@ipe.ac.cn
5 Fujian Longking Co., LTD, Longyan 364000, China; Huangxing@longking.com.cn
* Correspondence: lichangming@btbu.edu.cn (C.L.); yujian@ipe.ac.cn (J.Y.)

Received: 30 October 2020; Accepted: 21 November 2020; Published: 30 November 2020

Abstract: The development of efficient materials and processes is a long-term goal for the integrated flue gas purification in industry. In this study, a large-size V-based catalytic filter (L3000 mm × Φ150 mm) was prepared by loading the catalyst emulsion into a blank filter, which demonstrated excellent performance for simultaneously removing NO_x, SO_x and dust. The laboratory investigation found that the small catalytic particles, high catalyst loading and low face velocity could improve the $DeNO_x$ efficiency, and above 80% NO conversion could be achieved in the temperature range of 250–400 °C on the condition of <300 nm catalytic particle size, >7.41 wt % catalyst loading and <1.00 Nm/min face velocity. The negative effect of SO_2/H_2O was only observed below 300 °C, and the dust had little negative effects on $DeNO_x$ efficiency except for the increase of pressure drop. Moreover, a 90-day industrial test of 2380 catalytic filters over 100,000 Nm^3/h of flue gas (0.50 Nm/min) from a glass kiln demonstrated that the removal efficiency of both NO_x and SO_x could be maintained above 95% with great stability at 320–350 °C, and 99% dust could be removed with a pressure drop of less than 1.40 KPa. The results reported herein indicate the promising application prospect of large-size V-based catalytic filters for integrated flue gas purification in industry.

Keywords: NH_3-SCR; dedusting; catalytic filter; industrial application

1. Introduction

Selective reduction reaction with NH_3 (NH_3-SCR) has become one of the most promising methods to eliminate nitrogen oxides (NO_x) for decades, in which catalytic materials play a crucial role for the high removal efficiency of NO_x [1–3]. Currently, the V-based structured catalysts (honeycomb or plate-type) have been widely applied for both large-scale power plants and other small-medium boilers (e.g., coke oven, steel furnace and glass kiln) in the wide temperature range [4–6]. On the other hand, the toxic substances in flue gas (such as SO_x, alkali metals or alkaline earth metals), especially for the complex flue gas conditions of small-medium boilers, may cause severe poisoning of catalysts and shorten their lifetime [7–10]. Therefore, the development of new materials and processes is still of great significance to improve the removal efficiency as well as decrease the total cost for flue gas purification.

Integrated flue gas purification process based on catalytic filter material has attracted great attention in recent years due to its ability to remove NO_x, SO_x and dust simultaneously with a shortened process and reduced equipment investment [11–16]. The dust, as well as the waste desulfurizer, are filtrated and separated by an external surface membrane of a catalytic filter, and the NO_x is subsequently eliminated by SCR reaction over the catalyst inside the filter. Up to now, great progress has been achieved for the development of an effective catalytic filter with high catalytic activity and low-pressure drop. Different active components including Cu- [17,18], V- [19–21], Fe-based [22] catalytic filters as well as different blank filter materials [23] have been tried to improve their removal efficiency based on small filter samples (L500 mm × Φ60 mm) in the lab. Our previous work also developed a highly active V-based catalyst loaded in different ceramic filters [24], which displayed above 90% NO conversion in the temperature range of 250–450 °C. In particular, pilot tests of small-size catalytic filters (L1500 mm × Φ60 mm) were also done by Heidenreich [14], indicating the promising industrial application prospect of the catalytic filter. However, the treatment capacity of the small-size catalytic filter (L1500 mm × Φ60 mm) is too low to be widely used in industry due to its high equipment/engineering cost.

To extend the industrial application of catalytic filters, a large-size blank filter (L3000 mm × Φ150 mm) has been developed by many manufacturers. The wall thickness also increases from 10 mm (small filter) to 20 mm (large-size filter) to achieve enough strength/tenacity with a reduced risk of breaking off. Thus, the technical parameters of the large-size catalytic filter, such as catalyst loading, face velocity, as well as activity temperature range, may be different from the small catalytic filter. Moreover, the blank filter from different manufacturers may also have a different purifying effect. Currently, most research has focused on either improving the NO conversion or widening the temperature window [15,25,26], but little detailed data can be found about the denitration and dedusting behavior of the large-size catalytic filter in either lab or industrial occasions.

In the present work, a large-size V-based catalytic filter (L3000 mm × Φ150 mm) was prepared by loading the catalyst emulsion into a blank filter. The catalytic particle size of the catalyst emulsion, catalyst loading, and face velocity were investigated to improve the catalytic efficiency, and the interplay between the $DeNO_x$ and dedusting of the catalytic filter was also evaluated in the lab. Moreover, industrial tests were carried out in a glass kiln to assess the stability of the large-size catalytic filter for long-term use.

2. Results and Discussions

2.1. Characteristics of Materials

2.1.1. Composition and Structure of Powdery Catalyst

Figure 1A shows the XRD result of the powdery catalyst. It is shown that mainly TiO_2 was able to be detected by the device (denoted as triangle marks); the weak peak at about 20° could be assigned to the VO_x species, probably owing to its high loading on TiO_2. Figure 1B displays the type IV N_2 adsorption–desorption isotherms, which possessed an H_3-type hysteresis loop, revealing the mesoporous characteristics of catalyst. The corresponding pore size distribution of the catalyst was mainly between 1 nm and 100 nm, as shown in Figure 1C. The specific surface and average pore diameter of the powdery catalyst were 159 m^2/g and 9.2 nm, respectively. Figure 1D presents the SEM image, displaying the fine catalyst particles and fine arrangement. The good dispersal of active components, as well as the high specific surface of the catalyst, may have facilitated the improvement of its $DeNO_x$ efficiency.

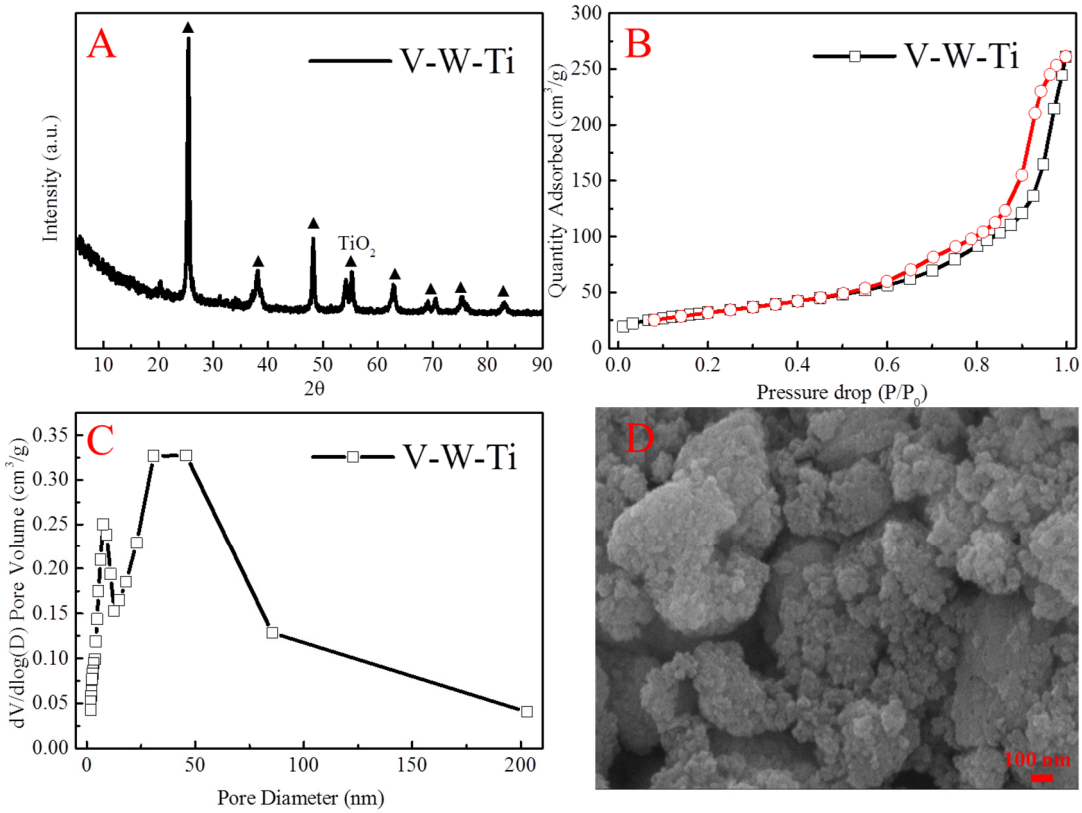

Figure 1. The structure of the powdery catalyst: (**A**) XRD pattern, (**B**) N_2 adsorption–desorption isotherms curve and (**C**) the corresponding pore size distribution together with (**D**) the SEM image.

2.1.2. Structure and Morphology of Catalytic Filter and Glass Ash

The XRF result of the blank filter (Table 1) shows the presence of three main oxides such as SiO_2 (61.93 wt %), Al_2O_3 (35.18 wt %) and TiO_2 (2.26 wt %). The catalytic filter contained six oxides after the addition of the V-W-Ti catalyst. Other trace elements, such as Zr, P, Ga, Cl, Ni, etc., were lower than 0.1 wt % and not listed. Compared with the blank filter, the pore size of the catalytic filter was reduced, indicating that the catalyst particles were coated into the filter. The pore volume and porosity of the two filters remained almost the same, indicating that the catalyst particles were well distributed on the surface of filter fibers, and the coated catalysts may have had negligible effects on the pressure drop of the filter.

Table 1. Composition as well as the pore parameters of blank filter and corresponding catalytic filter.

Sample	Composition (wt %)					Pore Volume ($cm^3 \cdot g^{-1}$)	Pore Diameter (nm)	Porosity (%)
	SiO_2	Al_2O_3	TiO_2	V_2O_5	WO_3			
Blank filter	61.93	35.18	2.26	-	-	1.14	446.4	71.04
Catalytic filter	47.94	35.33	12.66	2.65	0.62	1.13	401.6	69.42

Figure 2A,B shows SEM images of the blank filter and catalytic filter, respectively. There was little difference except that the fiber of the catalytic filter was rougher than that in the blank filter due to the coated catalysts. The results demonstrated that the catalyst particles were well dispersed and adhered on the surface of the filter fiber, which was consistent with the result of the pore structure of filters in Table 1. The SEM image of glass ash in Figure 2C shows the ash particles were about 4 μm, and its high magnification image (Figure 2D) displays the spherical ash particles were densely packed.

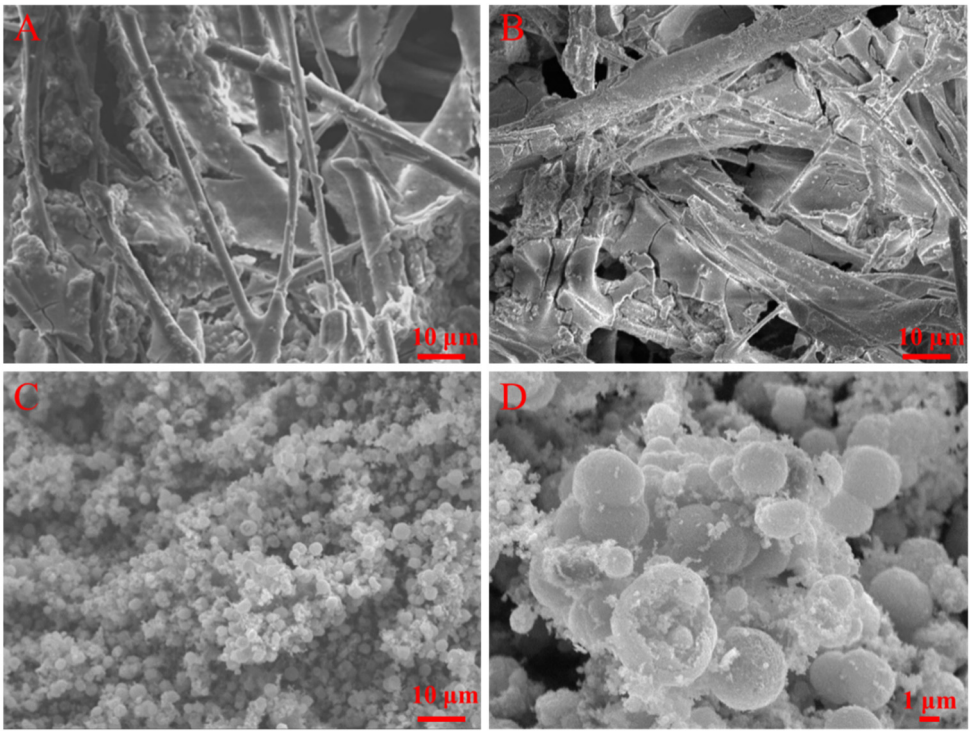

Figure 2. The SEM morphology of (**A**) blank filter, (**B**) catalytic filter, (**C**) glass ash at low magnification and (**D**) glass ash at high magnification.

2.1.3. Main Features of Glass Ash

The particle size distribution and chemical composition of glass ash are provided in Table 2. The X_{50} of the glass ash was 3.98 μm, which was consistent with the result of SEM presented in Figure 2. The XRF result showed that K_2SO_4, $ZnSO_4$ and $CaSO_4$ were the main chemical composition of glass ash. Generally, it was accepted that the alkali metals such as K, Ca, Na, etc., could easily react with the major active components of catalysts during SCR reaction, resulting in the decrease in surface area and catalytic activity [8–10,27,28]. Particularly, the high K and Ca content in glass ash was the main factor to limit the application of traditional honeycomb $DeNO_x$ process in glass or cement industries owing to the easy catalyst poisoning [10].

Table 2. The particle size distribution and chemical composition of glass ash based on the laser particle size analyzer (LPSA) and X-ray fluorescence (XRF) results.

Particle Size Distribution		Chemical Composition: Main Components			
X_{10} (μm)	0.58	SO_3 (wt %)	45.04	CaO (wt %)	4.53
X_{50} (μm)	3.98	K_2O (wt %)	33.54	SiO_2 (wt %)	3.22
X_{90} (μm)	16.25	ZnO (wt %)	6.80	PbO (wt %)	2.67

2.2. Laboratory Test

2.2.1. The Effect of Particle Size of Catalytic Emulsion

The effect of particle size on catalytic activity is displayed in Figure 3. Figure 3A shows the particle size accumulation curves of the three different emulsions. Emulsion C had the biggest particle size following by emulsion B and finally emulsion A with much finer particles. Figure 3B shows the NO conversion and N_2O concentration of different catalytic filters derived from emulsion A, B and C. Emulsion A with fine particles had the best NO conversion and the lowest N_2O concentration, followed by emulsion B with moderate NO conversion and moderate N_2O concentration. Lastly, emulsion C with

the lowest NO conversion among the three emulsions and possessed the highest N_2O concentration. The smaller the particle size of the catalytic emulsion, the higher the $DeNO_x$ activity. The fine particle size of the emulsion could facilitate the dispersion and exposure of active sites after coating the emulsion into the blank filter.

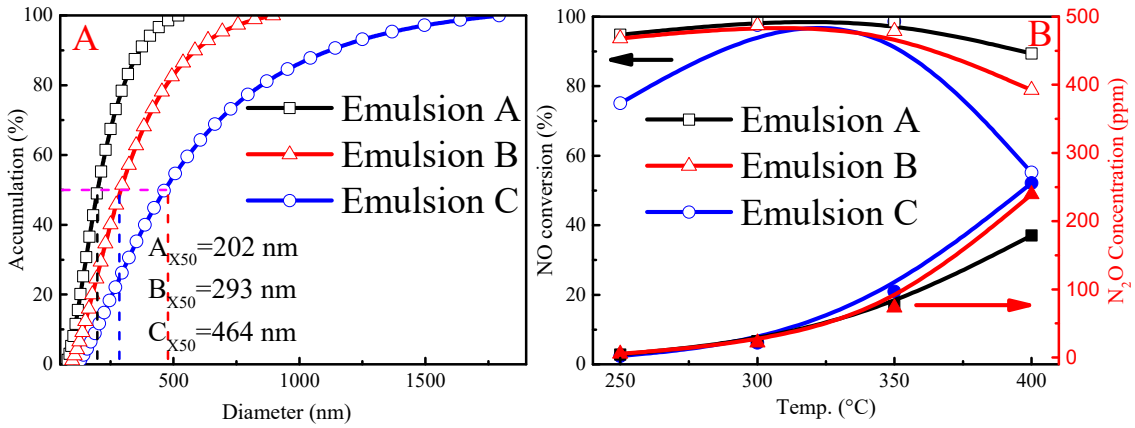

Figure 3. The (**A**) particle size accumulation curves of catalytic emulsion and (**B**) its effect on $DeNO_x$ performance of the catalytic filter.

2.2.2. The Effect of Catalyst Loading

NO conversion efficiency was determined by some substantial factors, including the catalyst loading. Figure 4A illustrates three filters with different catalyst loading, in which 5.74 wt % had the least catalyst loading, least NO conversion and lowest N_2O concentration at the temperature range of 250–400 °C. Improvement in $DeNO_x$ efficiency could be seen with an increase in catalyst loading but at the cost of increased N_2O concentration. Catalyst loading of 7.41 wt % reached its highest NO conversion efficiency of 98% with the formation of 151 ppm N_2O at 350 °C. The catalytic filter with the highest catalyst loading of 8.99 wt % obtained the highest NO conversion efficiency, also with the highest N_2O concentration. The pressure drop relative to catalyst loading is depicted in Figure 4B. The 8.99 wt % catalyst loading possessed the highest pressure with about 1.18 KPa at 250 °C and 1.4 KPa at 400 °C. The 5.74 wt % catalyst loading had the least pressure drop with 1.04 KPa at 250 °C and 1.2 KPa at 400 °C. The higher the catalyst loading on the catalytic filter, the higher the pressure drop was observed. These results indicated that NO conversion increased with the increase of the catalyst loading but at the expense of increased N_2O as well as pressure drop. Therefore, an appropriate catalyst loading should be selected in the practical industrial applications. In this investigation, catalyst loading of about 7.41 wt % was chosen for the following test.

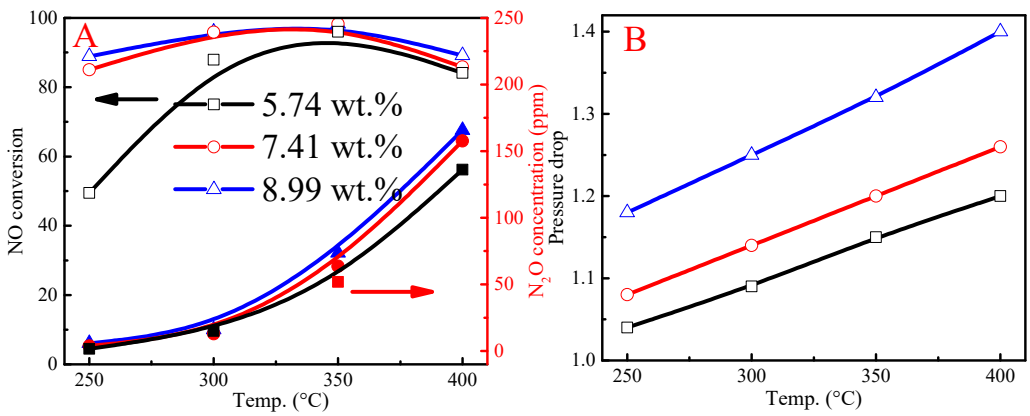

Figure 4. The effect of catalyst loading on (**A**) $DeNO_x$ performance and (**B**) pressure drop over the catalytic filter.

2.2.3. The Effect of Face Velocity

Face velocity is another important factor affecting the catalytic performance of the filter. Figure 5 profiles the effect of face velocity on $DeNO_x$ performance and pressure drop over the catalytic filter. As can be seen, the face velocity varied between 0.50 Nm/min and 1.50 Nm/min. In Figure 5A, face velocity of 0.5 Nm/min had the highest NO conversion efficiency and the highest N_2O concentration followed by 0.75 Nm/min, next 1.00 Nm/min and lastly 1.50 Nm/min face velocity with both the lowest NO conversion and N_2O concentration. The face velocity had the capability of altering the residence time of the flue gas through the filter. High face velocity means short residence, resulting in low NO conversion. Figure 5B gives the relationship between pressure drop and face velocity. The face velocity of 1.50 Nm/min had the highest pressure drop, which was because of the highest face velocity. Meanwhile, the pressure drop also increased with temperature, which was consistent with Darcy's law. Therefore, a suitable face velocity should be chosen according to the activity, pressure drop and economy in the practical industrial applications.

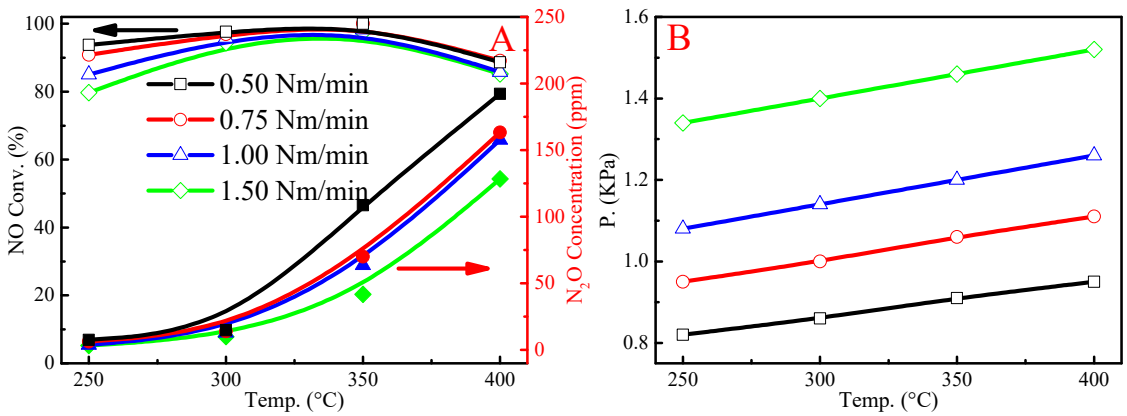

Figure 5. The effect of face velocity on (**A**) $DeNO_x$ performance and (**B**) pressure drop over a catalytic filter.

2.2.4. The Effect of H_2O and SO_2

As the exhaust usually contains a large amount of water vapor and SO_2, the effects of H_2O and SO_2 on the $DeNO_x$ performance of the catalytic filter were investigated and presented in Figure 6. It can be observed that the addition of H_2O notably weakened the NO conversion below 250 °C, which was ascribed to the severe competitive adsorption of H_2O and NH_3 at low temperatures [29,30]. As the temperature increased, the inhibition effect of H_2O decreased and even enhanced the NO conversion above 300 °C. Notably, the dramatic decrease of N_2O concentration observed, indicating the addition of H_2O restrains the oxidation of NH_3 at high temperature [22,31]. These results indicate that the presence of H_2O in the real flue gas may have dramatically weakened the undesirable oxidation of NH_3 and promoted the SCR selectivity.

As for SO_2, there was just a slight decrease in NO conversion with the introduction of 300 ppm SO_2. However, the addition of H_2O and SO_2 slightly decreased the activity at low temperatures when compared to the introduction of H_2O alone, which may be related to the formation of ammonium sulfate in the presence of both H_2O and SO_2 at 250 °C [32]. As the temperature increased, the SCR performance increased gradually, and then it was almost similar to that of introducing H_2O alone above 300 °C, signifying that the negative effect of H_2O/SO_2 could be neglectful above 300 °C. The demonstrated high SCR activity of catalytic filter and its great resistance of H_2O/SO_2 gives it of great application feasibility in industry.

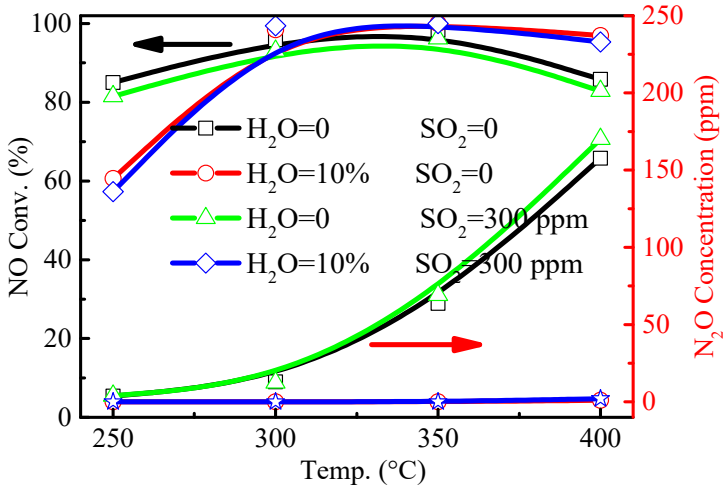

Figure 6. The effect of H_2O/SO_2 on NO conversion and N_2O concentration of catalytic filter.

2.2.5. Simultaneous Removal Efficiency of NO and Glass Ash

To further investigate the effect of glass ash, the SCR performance of catalytic filter against time in the presence of glass ash is given in Figure 7. Figure 7A shows the NO conversion and the removal efficiency of glass ash. It can be observed that the NO conversion fluctuated between 96% and 99% against the time series from 0 to 180 min, which presumably resulted from the dropping of glass ash from the filter surface after enough thickness of ash accumulated [33,34]. Nevertheless, the removal efficiency of glass ash remained nearly 100%, which was consistent with the previous report [23]. In Figure 7B, a pressure drop was also recorded during the simultaneous removal of NO and glass ash. It was noticeable that the pressure drop increased against the time series and reached a maximum level of more than 1.45 KPa. After blowback with compressed air, it returned to 1.30 KPa. The pressure drop was slightly higher than the initial value because some glass ash still covered the surface of the catalytic filter and could not be completely removed after the blowback [35]. This behavior was noticed throughout the entire 180 min with good repeatability. The results of the influence of ash will have great guiding significance for the stable operation of catalytic filters in industry.

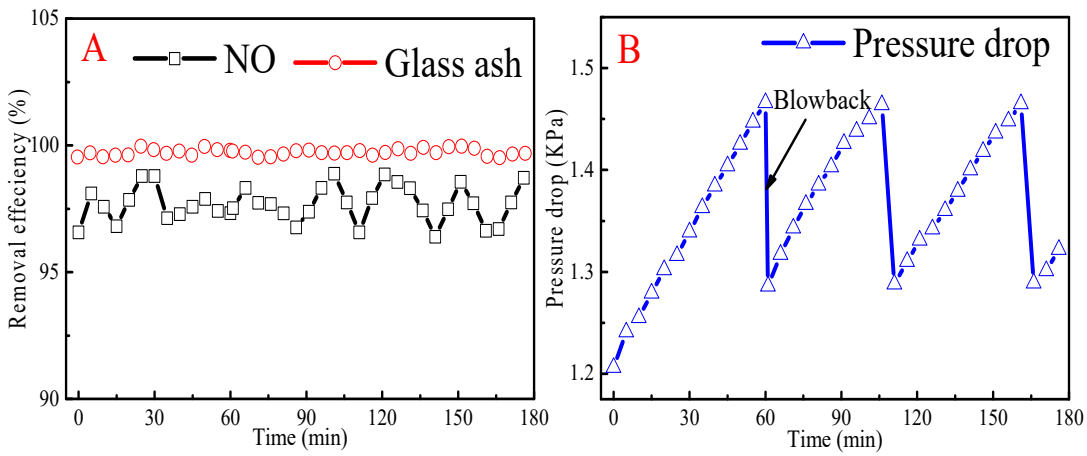

Figure 7. The (**A**) removal efficiency of NO and glass ash together with (**B**) the corresponding pressure drop during the process of removing NO and ash simultaneously.

2.3. Industrial Application

To validate the industrial applicability of the lab-scale results, 2380 large-size V-based catalytic filter (L3000 mm × Φ150 mm) with optimized parameters (catalytic emulsion of A_{X50} = 202 nm, ~7.5 wt % catalyst loading) were applied in the glass kiln. The basic process and apparatus diagram of the industrial

test are provided in Figure 8, which mainly included the ammonia injection, dry desulfurization, compressed air system and sampling system. As shown in the diagram, lime and NH_3 were introduced as desulfurizers and SCR reducing agent, respectively. The process of $DeNO_x$ and dedusting was carried out simultaneously by a catalytic filter in the sampling system. At the same time, the compressed air was used to blow back the catalytic filter. The SO_2 presented in the flue gas could react with lime to form solid particles. The solid particles and glass ash were later separated by the filter and then deposited in the preserved area below the sampling system. Meanwhile, NO_x in the flue gas reacted with NH_3 through the catalytic filter in the sampling system, and the gas was subsequently cleaned and out to the atmosphere through the chimney.

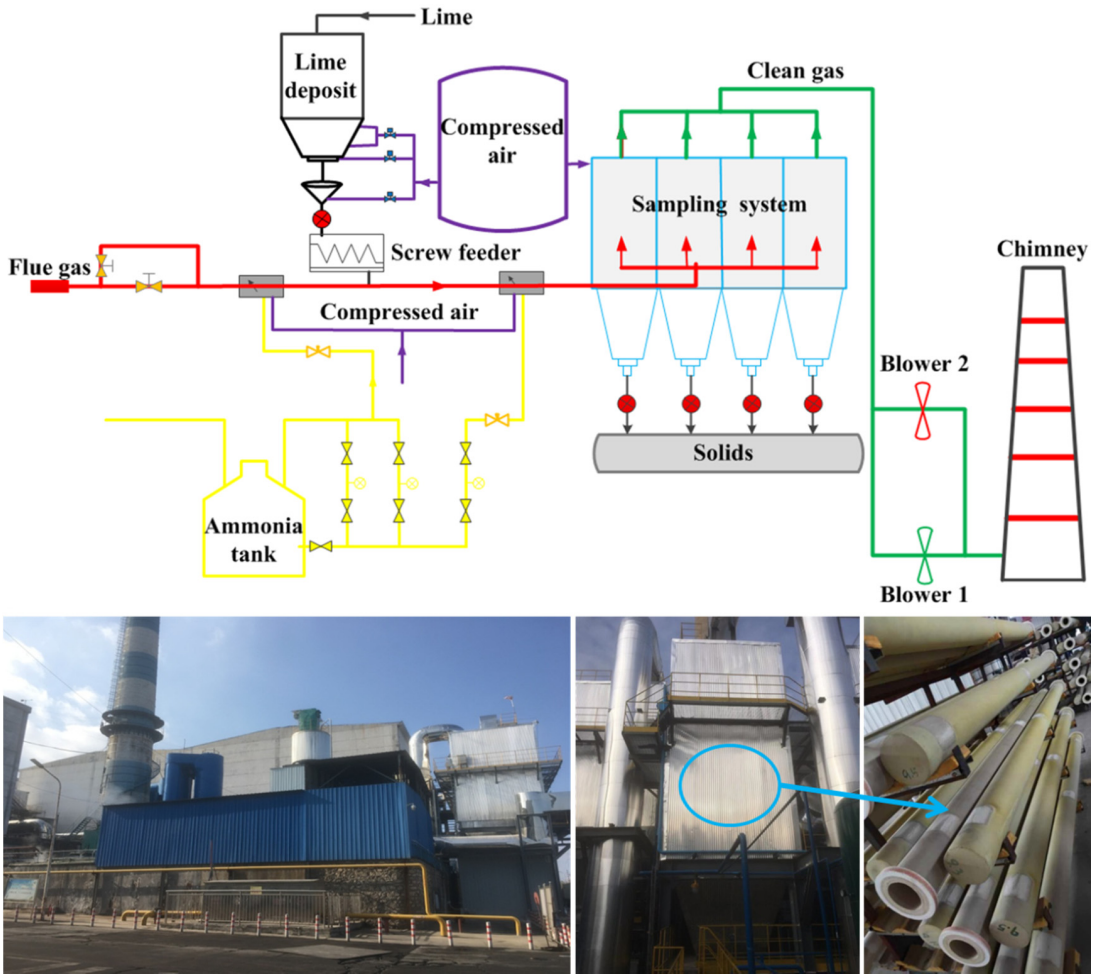

Figure 8. The basic process and apparatus diagram of the industrial application for the large-size catalytic filter in a glass kiln.

The evaluation of the removal efficiency of pollutants and the corresponding pressure drop with time in the temperature range of 320–350 °C are displayed in Figure 9. The $DeNO_x$ efficiency fluctuated between 96% and 99%, the SO_x conversion was more than 95%, and nearly 100% removal efficiency of glass ash was achieved in the whole day of the test evaluation. As for the pressure drop, it varied between 1.30 and 1.36 KPa as time passed. The fluctuation of removal efficiency and pressure drop within the 90 days was owing to the inevitable change of flue gas conditions, but the industrial test results still confirm that our catalytic filter was effective and stable for the integrated purification of flue gas from glass kiln in industry.

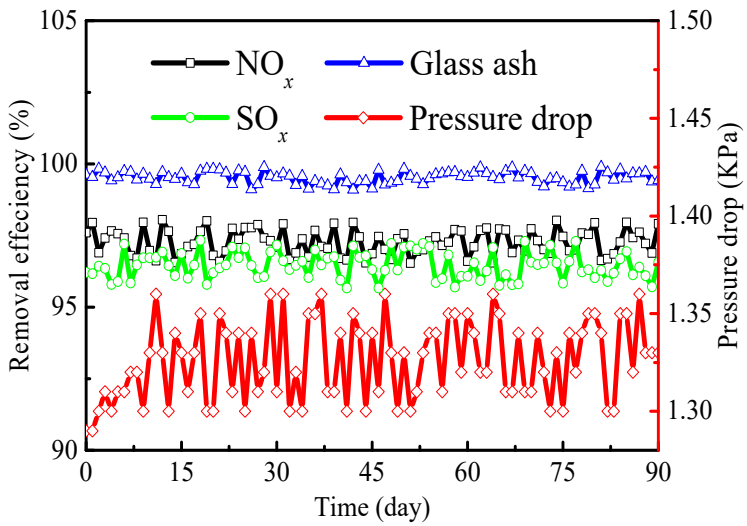

Figure 9. The removal efficiency of NO_x, SO_x and glass ash together with the pressure drop during the 90-day industrial test (daily average).

The detailed data of pollutants before and after purification by the catalytic filter during the industrial application are illustrated in Table 3. The inlet concentration of NO_x was 2400–2600 mg/Nm^{3,} and the outlet concentration after the gas purification was less than 100 mg/Nm^3. The inlet concentration of SO_x was about 2800–3100 mg/Nm^{3,} and the outlet was less than 150 mg/Nm^3. The amount of 360–420 mg/Nm^3 of glass ash from the inlet was reduced to less than 5 mg/Nm^3 in the outlet. These results demonstrate the powerful capacity of the catalytic filter for the integrated purification of flue gas with a high concentration of pollutants.

Table 3. The detailed data of flue gas before and after purification by the catalytic filter during the industrial test.

Items	Inlet	Outlet
NO_x	2400–2800 mg/Nm^3	<100 mg/Nm^3
SO_x	2800–3100 mg/Nm^3	<150 mg/Nm^3
Glass ash	360–420 mg/Nm^3	<5 mg/Nm^3
H_2O	10–15 vol %	10–15 vol %
O_2	9–11 vol %	9–11 vol %

3. Experimental Section

3.1. The Preparation of Catalyst and Catalytic Filter

The catalytic emulsion was prepared by mixing raw V, W, Ti salt precursors for coating the blank filter. To increase the adhesion between the catalyst and blank filter, some aluminum sol was added to the emulsion. The powdery catalyst was obtained after drying the emulsion, and then it was calcined at 400 °C for 5 h for catalyst characterization. The detailed coating process of a large-size catalytic filter can be found in our previous patent with the method of spraying the catalytic emulsion from the inside of the rotating blank filter, which can effectively avoid the blockage of the filter channel. The solid content of catalytic emulsion was about 5 wt %, and the original dimension of the blank filter element was 3000 mm in length and 110/150 mm inner/outer diameter from Fujian Longking Co., LTD. After the blank filter was coated with the desired catalyst loading, it was dried at 120 °C for 3 h and calcined at 400 °C for 5 h to obtain a catalytic filter for industrial application. Meanwhile, to evaluate the $DeNO_x$ activity of the catalytic filter in the lab, it was cut into 30 mm length to fit the experimental reactor.

3.2. Catalyst Characterization

An X-ray fluorescence (XRF) spectrometer (AXIOS-MAX, PANalytical B.V, Almelo, The Netherlands) was used to determine the chemical composition of catalysts. X-ray diffraction (XRD) patterns were recorded on an X-ray diffractometer (Empyrean, PANalytical B.V, Almelo, The Netherlands) in the 2θ range of 5–90° operating at 40 kV and 40 mA using Cu Kα radiation. The nitrogen adsorption–desorption apparatus (ASAP 2020, Micromeritics Instrument Corp, Atlanta, GA, USA) was used to determine the pore size distribution and surface area of powdery catalyst at 77 K. Sample was degassed at 200 °C for 10 h with the mass of 0.1 g before the measurement. The thermal analysis experiment was performed on TG/DTA 6300 produced by NSK. The sample (5 mg) was placed in the crucible and heated from 30 °C to 700 °C at a rate of 10 °C/min under N_2 atmosphere. The pore structure of the filters was characterized using a mercury instrument (AutoPore 9510, Micromeritics, Atlanta, GA, USA). Microstructure and morphology of the samples were recorded on SU8020 scanning electron microscope (SEM, HITACHI, Tokyo, Japan). A laser particle size analyzer (LS13320, Beckman Coulter, Brea, CA, USA) was used to characterize the particle size of the glass ash. The particle size distribution of catalytic emulsion was carried out at nanometer particle size analyzer (DelsaNano C, Beckman Coulter, Brea, CA, USA), and the X_{50} is the ratio when the accumulated particle number below a specific particle size occupy half the total particle number.

3.3. Performance Test

A self-designed steel experimental apparatus (Figure 10) was used to conduct the catalytic activity of the catalytic filter in the lab-scale (L30 mm × Φ150 mm). Graphite slices were used to prevent gas leakage prior to the fix with flange, threaded cap and threaded rod. Before the simulated flue gas was introduced into the reactor, it was preheated and then passed through the catalytic filter from the outer to the inner part. The pressure difference between the inner and outer of the catalytic filter was measured by a pressure gauge. The glass ash was introduced through a screw feeder at a rate of 500 mg/Nm^{3,} and the collection efficiency of dust was calculated by the weighing method. After the pressure drop reaches a certain value with the accumulation of glass ash on the outside of the filter, the process of blowback with compressed air would be introduced from inner to outer (catalytic filter) to clear away the glass ash and lower down the pressure drop to a stable value. The simulated flue gas consisted of 700 ppm NO, 700 ppm NH_3, 5 vol % O_2, 10 vol % H_2O (when used), 300 ppm SO_2 (when used), and balanced with N_2 at the face velocity from 0.50 Nm/min to 1.50 Nm/min. An online portable FT-IR analyzer (Gasmet DX4000, Finland) was used to constantly monitor the concentration of NO_x and SO_2 in/out the flue gas.

Figure 10. Lab-scale test reactor for a catalytic filter.

The industrial test of a large-size V-based catalytic filter (L3000 mm × Φ150 mm) was carried out in the glass kiln, as shown in Figure 8. The flow rate during the industrial application was about 100,000 Nm^3/h (0.50 Nm/min), and the operating temperature ranged from 320 °C to 350 °C in the sampling system. The concentration of SO_x, as well as glass ash in the original flue gas, was in the range of 2800–3100 mg/Nm^3 and 360–420 mg/Nm^3, respectively. The inlet concentration of NO_x was controlled from 2400 mg/Nm^3 to 2800 mg/Nm^3. Water vapor content was 10–15 vol % in the flue gas, and the O_2 concentration was about 10 vol %. In addition, the concentration of pollutants in the outlet was monitored and recorded online. The results (daily average) of the test for 90 days are reported in this investigation.

The NO conversion, N_2O concentration and face velocity were calculated according to the following equations:

$$\text{NO conversion} = \frac{[\text{NO}]_{in} - [\text{NO}]_{out}}{[\text{NO}]_{in}} \times 100\% \quad (1)$$

$$\text{N}_2\text{O concentration} = [\text{N}_2\text{O}]_{out} - [\text{N}_2\text{O}]_{in} \quad (2)$$

$$\text{Face velocity} = \frac{V}{PI \times D \times L} \quad (3)$$

where $[NO]_{in}$ and $[NO]_{out}$ stand for the concentration of NO in the inlet and outlet gas, respectively. Face velocity is the flow of flue gas through per filtering area in unit time. V (m^3/min) represents the volume of the passed flue gas per minute, D (m) is the average diameter of the catalytic filter and L (m) stands for the length of the catalytic filter.

4. Conclusions

In summary, the large-size V-based catalytic filter (L3000 mm × Φ150 mm) was prepared through loading the catalyst emulsion into the blank filter, and its performance of the integrated flue gas purification was tested both in the lab and in glass kiln, which could achieve more than 90% NO conversion (>300 °C) in the presence of H_2O/SO_2 and nearly 100% collection efficiency of dust with the pressure drop lower than 1.40 KPa. It was observed that the fine particle size of catalytic emulsion, the increased catalyst loading as well as the low face velocity could improve catalytic $DeNO_x$ performance. Except for the gradually increased pressure drop, the introduction of glass ash had little effect on the $DeNO_x$ activity. Moreover, the blowback with compressed air could clear away the ash outside of the catalytic filter and lower down the pressure drop to a stable value. The 90-day industrial test demonstrated great stability and reliability for the application of catalytic filters in an industrial glass kiln. Particularly, the catalytic filter possessed a powerful capacity to deal with a high concentration of pollutants, and 2800–3100 mg/Nm^3 SO_x, 2400–2800 mg/Nm^3 NO_x and 360–420 mg/Nm^3 dust can be reduced to below 100 mg/Nm^3, 150 mg/Nm^3 and 5 mg/Nm^3, respectively. The demonstrated great performance for the integrated flue gas purification manifests the promising application prospect of the large-size V-based catalytic filter in industry.

Author Contributions: Data curation and writing—original draft, L.H.; writing—original draft, Z.C.; writing—review and editing, C.L.; investigation, X.Y.; formal analysis, Z.Y.; supervision, G.X.; Conceptualization and Funding acquisition, S.G.; methodology, X.H.; project administration and Resources, J.Y. All authors have read and agreed to the published version of the manuscript.

Funding: This work was supported by the Natural Science Foundation of China (Grant 21601192 and 21878310), the National Key Research and Development Program of China (2017YFB0310403) and the Open Subject from State Key Laboratory of Multiphase Complex Systems (Grant MPCS-2019-0-03).

Conflicts of Interest: The authors declare that they have no conflict of interest.

References

1. Jung, H.; Park, E.; Kim, M.; Jurng, J. Pilot-scale evaluation of a novel TiO_2-supported V_2O_5 catalyst for $DeNO_x$ at low temperatures at a waste incinerator. *Waste Manag.* **2017**, *61*, 283–287. [CrossRef]
2. Yu, J.; Li, C.-M.; Guo, F.; Gao, S.-Q.; Zhang, Z.-G.; Matsuoka, K.; Xu, G.-W. The pilot demonstration of a honeycomb catalyst for the $DeNO_{(x)}$ of low-temperature flue gas from an industrial coking plant. *Fuel* **2018**, *219*, 37–49. [CrossRef]
3. Zhang, Y.-S.; Li, C.-M.; Wang, C.; Yu, J.; Xu, G.; Zhang, Z.-G.; Yang, Y.-Q. Pilot-scale test of a V_2O_5–WO_3/TiO_2-coated type of honeycomb $DeNO_x$ catalyst and its deactivation mechanism. *Ind. Eng. Chem. Res.* **2019**, *58*, 828–835. [CrossRef]
4. Svachula, J.; Ferlazzo, N.; Forzatti, P.; Tronconi, E.; Bregani, F. Selective reduction of nitrogen oxides (NO_x) by ammonia over honeycomb selective catalytic reduction catalysts. *Ind. Eng. Chem. Res.* **1993**, *32*, 1053–1060. [CrossRef]
5. Bahamonde, A.; Avila, P.; Beretta, A.; Tronconi, E. An experimental and theoretical investigation of the behavior of a monolithic Ti-V-W-sepiolite catalyst in the reduction of NO_x with NH_3. *Ind. Eng. Chem. Res.* **1996**, *35*, 2516–2521. [CrossRef]
6. Li, C.-M.; Yu, J.; He, Y.; Yu, C.; Li, P.; Wang, C.; Huangfu, L.; Gao, S.-Q. The industrial feasibility of low temperature $DeNO_x$ in the presence of SO_x: A project case in a medium coking plant. *RSC Adv.* **2018**, *8*, 18260–18265. [CrossRef]
7. Liu, Z.-M.; Zhang, S.-X.; Li, J.-H.; Zhu, J.-Z.; Ma, L.-L. Novel V_2O_5-CeO_2/TiO_2 catalyst with low vanadium loading for the selective catalytic reduction of NO_x by NH_3. *Appl. Catal. B Environ.* **2014**, *158*, 11–19. [CrossRef]
8. Fang, D.; Xie, J.-L.; Hu, H.; Zhang, Z.; He, F.; Zheng, Y.; Zhang, Q. Effects of precursors and preparation methods on the potassium deactivation of MnO_x/TiO_2 catalysts for NO removal. *Fuel Process. Technol.* **2015**, *134*, 465–472. [CrossRef]
9. Kong, M.; Liu, Q.-C.; Zhou, J.; Jiang, L.-J.; Tian, Y.-M.; Yang, J.; Ren, S.; Li, J.-L. Effect of different potassium species on the deactivation of V_2O_5-WO_3/TiO_2 SCR catalyst: Comparison of K_2SO_4, KCl and K_2O. *Chem. Eng. J.* **2018**, *348*, 637–643. [CrossRef]
10. Wang, C.; Li, C.-M.; Li, Y.-J.; Huangfu, L.; Liu, Z.-E.; Gao, S.-Q.; Yu, J. Destructive influence of cement dust on the structure and $DeNO_x$ performance of V-based SCR catalyst. *Ind. Eng. Chem. Res.* **2019**, *58*, 19847–19854. [CrossRef]
11. Saracco, G.; Specchia, V. Simultaneous removal of nitrogen oxides and fly-ash from coal-based power-plant flue gases. *Appl. Therm. Eng.* **1998**, *18*, 1025–1035. [CrossRef]
12. Fino, D.; Russo, N.; Saracco, G.; Specchia, V. A multifunctional filter for the simultaneous removal of fly-ash and NO_x from incinerator flue gases. *Chem. Eng. Sci.* **2004**, *59*, 5329–5336. [CrossRef]
13. Fino, D.; Russo, N.; Saracco, G.; Specchia, V. Multifunctional filter for treatment of the flue gases from municipal waste incinerators. *Ind. Eng. Chem. Res.* **2005**, *44*, 9542–9548. [CrossRef]
14. Heidenreich, S.; Nacken, M.; Hackel, M.; Schaub, G. Catalytic filter elements for combined particle separation and nitrogen oxides removal from gas streams. *Powder Technol.* **2008**, *180*, 86–90. [CrossRef]
15. Kim, Y.A.; Choi, J.H.; Scott, J.; Chiang, K.; Amal, R. Preparation of high porous Pt-V_2O_5-WO_3/TiO_2/SiC filter for simultaneous removal of NO and particulates. *Powder Technol.* **2008**, *180*, 79–85. [CrossRef]
16. Kang, M.; Park, E.D.; Kim, J.M.; Yie, J.E. Simultaneous removal of particulates and NO by the catalytic bag filter containing MnO_x catalysts. *Korean J. Chem. Eng.* **2009**, *26*, 86–89. [CrossRef]
17. Park, Y.O.; Lee, K.W.; Rhee, Y.W. Removal characteristics of nitrogen oxide of high temperature catalytic filters for simultaneous removal of fine particulate and NO_x. *J. Ind. Eng. Chem.* **2009**, *1*, 36–39. [CrossRef]
18. Zhang, Y.-S.; Li, C.-M.; Yu, C.; Tran, T.; Guo, F.; Yang, Y.-Q.; Yu, J.; Xu, G.-W. Synthesis, characterization and activity evaluation of Cu-based catalysts derived from layered double hydroxides (LDHs) for $DeNO_x$ reaction. *Chem. Eng. J.* **2017**, *330*, 1082–1090. [CrossRef]
19. Saracco, G.; Specchia, S.; Specchia, V. Catalytically modified fly-ash filters for NO_x reduction with NH_3. *Chem. Eng. Sci.* **1996**, *51*, 5289–5297. [CrossRef]
20. Nacken, M.; Heidenreich, S.; Hackel, M.; Schaub, G. Catalytic activation of ceramic filter elements for combined particle separation, NO_x removal and VOC total oxidation. *Appl. Catal. B Environ.* **2007**, *70*, 370–376. [CrossRef]

21. Zhang, Y.-S.; Li, C.-M.; Zeng, H.; Yu, C.; Yu, J.; Yang, Y.-Q.; Xu, G.-W.; Gao, S.-Q. Preparation of V_2O_5-WO_3-TiO_2/cordierite based catalytic filter for removal of NO_x from flue gas. *Chin. J. Process. Eng.* **2017**, *17*, 1249–1256.
22. Huangfu, L.; Abubakar, A.; Li, C.-M.; Li, Y.-J.; Wang, C.; Gao, S.-Q.; Liu, Z.-E.; Yu, J. Development of red mud coated catalytic filter for NO_x removal in the high temperature range of 300–450 °C. *Catal. Lett.* **2020**, *150*, 702–712. [CrossRef]
23. Heidenreich, S. Hot gas filtration-A review. *Fuel* **2013**, *104*, 83–94. [CrossRef]
24. Yu, C.; Li, C.-M.; Zhang, Y.-S.; Guo, F.; Yu, J.; Yang, Y.-Q.; Xu, G.-W. The effect of ceramic matrices on the dispersion of loaded catalyst and the deNO_x activity of catalytic filters. *J. Chem. Ind. Eng.* **2018**, *69*, 682–689.
25. Choi, J.H.; Kim, J.H.; Bak, Y.C.; Amal, R.; Scott, J. Pt-V_2O_5-WO_3/TiO_2 catalysts supported on SiC filter for NO reduction at low temperature. *Korean J. Chem. Eng.* **2005**, *22*, 844–851. [CrossRef]
26. Kim, Y.; Choi, J.; Yu, L.; Bak, Y. Modification of V_2O_5-WO_3/TiO_2 catalysts supported on SiC filter for NO reduction at low temperature. *Adv. Nanomater. Process.* **2007**, *124*, 1713.
27. Fang, D.; He, F.; Xie, J.; Dong, P. Influence of sodium on MnO_x/TiO_2 catalysts for SCR of NO with NH_3 at low temperature. *Mater. Res. Innov.* **2014**, *18*, 45–49. [CrossRef]
28. Li, X.; Li, X.-S.; Yang, R.-T.; Mo, J.; Li, J.; Hao, J. The poisoning effects of calcium on V_2O_5-WO_3/TiO_2 catalyst for the SCR reaction: Comparison of different forms of calcium. *Mol. Catal.* **2017**, *434*, 16. [CrossRef]
29. Yang, S.-J.; Wang, C.-Z.; Chen, J.-H.; Peng, Y.; Ma, L.; Chang, H.-Z.; Chen, L.; Liu, C.-X.; Xu, J.-Y.; Li, J.-H.; et al. A novel magnetic Fe-Ti-V spinel catalyst for the selective catalytic reduction of NO with NH_3 in a broad temperature range. *Catal. Sci. Technol.* **2012**, *2*, 915–917. [CrossRef]
30. Yang, S.-J.; Liu, C.-X.; Chang, H.-Z.; Ma, L.; Qu, Z.; Yan, N.-Q.; Wang, C.-Z.; Li, J.-H. Improvement of the activity of gamma-Fe_2O_3 for the selective catalytic reduction of no with NH_3 at high temperatures: NO reduction versus NH_3 oxidization. *Ind. Eng. Chem. Res.* **2013**, *52*, 5601–5610. [CrossRef]
31. Huangfu, L.; Abubakar, A.; Li, C.-M.; Li, Y.-J.; Wang, C.; Yu, J.; Gao, S.-Q. The utilization of red mud waste as industrial honeycomb catalyst for selective catalytic reduction of NO. *R. Soc. Open Sci.* **2019**, *6*, 191183. [CrossRef] [PubMed]
32. Gan, L.-N.; Guo, F.; Yu, J.; Xu, G.-W. Improved low-temperature activity of V_2O_5-WO_3/TiO_2 for denitration using different vanadium precursors. *Catalysts* **2016**, *6*, 25. [CrossRef]
33. Lee, J.S.; Shin, K.H.; Shin, M.C.; Cho, D.H.; Lee, H.-S. Properties of catalytic filter for the hot gas cleaning. *Mater. Sci. Forum* **2004**, *4*, 1181–1184. [CrossRef]
34. Kanaoka, C.; Amornkitbamrung, M. Effect of filter permeability on the release of captured dust from a rigid ceramic filter surface. *Powder Technol.* **2001**, *118*, 113–120. [CrossRef]
35. Heidenreich, S.; Scheibner, B. Hot gas filtration with ceramic filters: Experiences and new developments. *Filtr. Sep.* **2002**, *39*, 22–25. [CrossRef]

Publisher's Note: MDPI stays neutral with regard to jurisdictional claims in published maps and institutional affiliations.

© 2020 by the authors. Licensee MDPI, Basel, Switzerland. This article is an open access article distributed under the terms and conditions of the Creative Commons Attribution (CC BY) license (http://creativecommons.org/licenses/by/4.0/).